# Bandwidth Enhancement of Microstrip Patch Antenna Using Metasurface

Felipe Ferreira de Araújo[1] , Antonio Luiz Pereira de Siqueira Campos[1] , Ruann Victor de Andrade Lira[1] , Alfredo Gomes Neto[2] , Adaildo Gomes d'Assunção[1]

*[1] Federal University of Rio Grande do Norte, Av. Senador Salgado Filho, 3000, Natal, RN, Brazil,*
*alpscampos@gmail.com*
*[2]Federal Institute of Paraíba, Av Primeiro de Maio, 720, Jaguaribe, João Pessoa, PB, Brazil,*
*alfredogomesjpa@gmail.com*

*Abstract*— **In this article, bandwidth enhancement of a microstrip patch antenna using a new kind of metasurface is discussed. This new geometry is used to generate new resonances in antenna and with an optimal position of the metasurface in relation to antenna we can overlap the resonances and obtain a large bandwidth. The proposed antenna showed a bandwidth from 5.1 GHz to 8.0 GHz what can it able to be applied in WiFi 5 and 6. Numerical results were obtained with Ansys HFSS software. A prototype was built and measurements for $S_{11}$, Smith chart and gain were performed. Numerical and experimental results are in good agreement.**

*Index Terms*— Patch Antenna, Metasurface, Bandwidth Enhancement.

## I. INTRODUCTION

Microstrip antennas are being widely used in wireless communications due to their low profile, weight and manufacturing cost [1], [2]. In addition, these antennas can be easily integrated into electronic circuits. Despite these interesting advantages, this type of antenna has some disadvantages, such as narrow bandwidth, low efficiency, and low power operation, among others. Depending on the application, bandwidth may be an impediment to use this type of antenna.

The fractional bandwidth of a microstrip antenna usually ranges from 1 to 5 % [1]. This contrasts with fractional bandwidths of 15 to 50 % of other antennas, such as dipoles, slot antennas, and horn-type waveguide antennas [3], [4]. To overcome bandwidth limitations, some design techniques may be employed.

The bandwidth of microstrip antenna can be augmented through use of dielectric resonators (DRs), made using low loss materials with high permittivity [5]. The technique of increasing losses is not recommended when power is limited, as it is the case with portable or mobile communications equipment, as this may reduce their radiation efficiency.

Another alternative is increase the substrate thickness or multi-layers' structures [6]. However, in many applications, such as cell phones, the space available for antenna accommodation is limited, which restricts the volume occupied by the antenna.

Another approach involves the coupling of electromagnetic band-gap (EBG) structures to the patch

of microstrip antennas [7]. In recent years, patch antennas have been incorporated with EBG structures to improve surface wave suppression antenna performance, and are used as a ground plane [8], [9].

As an alternative to some limitations of the mentioned methods, the use of metasurfaces can be highlighted. Metasurfaces are typically two-dimensional arrays of small scatters or apertures in order to achieve some desirable electromagnetic behavior [10], [11]. The metasurface desired property is usually one that is not found in nature (negative permittivity and permeability, near-zero refractive index).

This work proposes a microstrip antenna coupled to a metasurface capable of operating in the WiFi 5 (5.15 – 5.725 GHz) and 6 (5.925 – 7.125 GHz) bands. To make the antenna more compact and low profile, the patch and metasurface are put in direct contact, thus eliminating the air gap between them. The aim is to achieve an antenna that operates from 5.1 GHz to 7.2 GHz with high gain in the entire band. The proposed structure is easy to build, inexpensive and compact compared to most previous configurations [6], [11] and has a higher bandwidth compared to [13], [15]. The results of the studies show that the metasurface characteristics and the unit cell pattern change the antenna impedance resulting in the overlapping of the new resonant frequencies, which allow a measured fractional bandwidth of 45.4 % (5.1 – 8.0 GHz).

## II. PREVIOUS WORKS

In [11], a broadband antenna coupled with a double-layered meta-surface is proposed. The metasurface consists of two metallic layers printed on two dielectric layers and each metallic layer contains an array of $4 \times 4$ square cells. The antenna is fed by coupling. This design makes the antenna work in two different operating modes, with resonant frequencies close to each other, increasing the bandwidth. The impedance bandwidth of $-10$ dB is about 43 % (from 4.08 to 6.38 GHz) and with a maximum realized gain of 11.6 dBi. The total size of the antenna is $65 \times 65$ mm$^2$ with a thickness of 5.03 mm.

In [12] an antenna combined with a fractal metasurface was proposed to increase bandwidth. The antenna patch is of the circular type with the insertion of four rectangular slots and six double rings on a FR4 substrate with 1.6 mm of thickness. The gain of the antenna is about 3.6 dB and 90 % efficiency with a size of $40 \times 40$ mm$^2$. The final bandwidth was $2.3 – 4.0$ GHz.

In [13] the authors proposed a hybrid metasurface (HMS) to form an array of broadband antennas. The antenna consists of a $4 \times 4$ matrix of square and metallic patches fed by a 50 $\Omega$ line through an H-shaped coupling slot on the ground plane. The total size of the array is $95 \times 95$ mm$^2$ with F4BTM substrate ($\varepsilon_r = 3.38$, loss tangent of 0.0027) and 4.08 mm of thickness. The measurement shows an impedance bandwidth of 28 % ($4.41 – 5.85$ GHz). The gain is 8.4 dBi in the operational band.

In [14], a low-profile microstrip antenna coupled with a metasurface as a ground plane was proposed. The metasurface is periodic with diamond-shaped unit cells. The antenna has a total size of

$55 \times 55$ mm$^2$ and 0.5 mm of thickness. The antenna has an impedance bandwidth of 1.83 %, radiation efficiency of 83 % in the measurement and a maximum gain of 4.6 dBi.

In [15], an antenna with potential application in satellite communications was developed by coupling a metasurface to a microstrip antenna. The metasurface basically consists of four unit cells with parasitic square crossed gaps in an array of $2 \times 2$ elements. The bandwidth was 39.25 % (4.28 – 6.37 GHz) and gain of 6.8 dBi. The total size of the antenna is $36 \times 36$ mm² on a FR4 substrate with a thickness of 3.5 mm.

In this work, we propose the use of a circular metasurface coupled to a patch antenna to increase bandwidth. The final volume of the antenna was approximately 3.82 cm$^3$. We rotate the metasurface with respect to the antenna, to obtain the largest possible bandwidth. The antenna can be used for WiFi 5 and 6 applications. The final fractional bandwidth was 45.4 % and the peak gain was 3.8 dBi. The fractional bandwidth is obtained for the $-10$ dB level of the $S_{11}$ parameter. The performances of the work cited in this section are compared in Table I. The results are compared in terms of bandwidth, gain and antenna dimensions.

TABLE I. COMPARISON OF RECENT ARTICLES PUBLISHED WITH BANDWIDTH ENHANCEMENT OF MICROSTRIP PATCH ANTENNA

| Reference number | Fractional bandwidth | Volume (cm$^3$) | Peak Gain (dBi) |
|---|---|---|---|
| [6] | 54 % | 5.04 | 7.2 |
| [11] | 43 % | 22.4 | 11.6 |
| [12] | 62 % | 2.56 | 3.6 |
| [13] | 28 % | 36.8 | 8.4 |
| [14] | 1.8 % | 1.51 | 4.6 |
| [15] | 39 % | 4.53 | 6.8 |
| This work | 45.4 % | 3.82 | 3.8 |

## III. PROPOSED PATCH ANTENNA AND METASURFACE

This section demonstrates the proposed antenna design step by step. A traditional patch antenna is manufactured and optimized for a good impedance matching and low production cost. The substrate is FR4 and circular in shape with radius of $R = 20$ mm ($\varepsilon_r = 4.4$) and thickness of h = 1.524 mm. The antenna patch is a square with dimension 21.6 mm x 21.6 mm and was based on the one proposed in [20]. Four "L" -shaped slots of arm lengths equal to Ly = 8.55 mm and width Ws1 = 1.0 mm are incorporated into the patch as shown in Fig. 1.
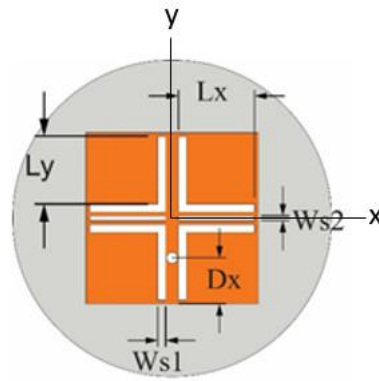
Fig. 1. Physical parameters of the proposed antenna.

To aid in bandwidth enhancement, new capacitive and inductive elements are inserted into the antenna patch through two more slots in the center position of the patch with width $W_{s2} = 0.6$ mm and length $L_x = 9.55$ mm, giving rise to a new resonant frequency in our bandwidth of interest, following modifications of the patch used in [20] as shown in Figs. 2 and 3. For antenna feed, a 50 Ω coaxial cable is connected via an SMA connector at a distance $D_x = 5.8$ mm from the Edge of square patch.
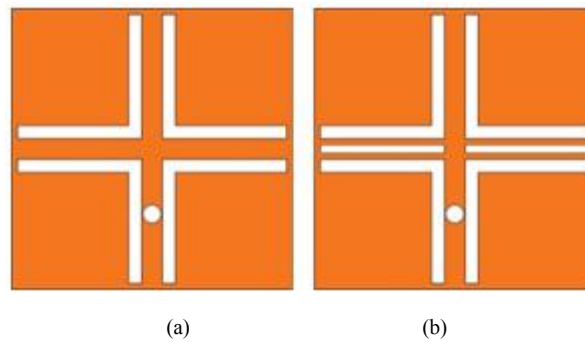
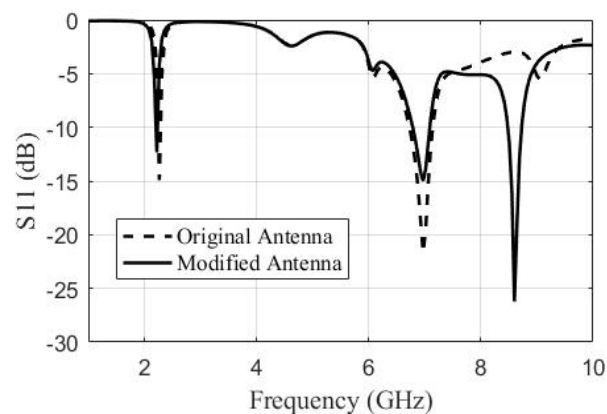Fig. 2. Microstip patch antenna: (a) used in [20] and (b) proposed in this work.

Fig. 3. Comparison between the |S11| of the proposed antenna in [20] and our antenna.

The proposed metasurface is composed of an arrangement of unit cells periodically allocated along the XY-plane. It was designed on FR4 substrate, relative permittivity $\varepsilon_r = 4.4$, with single conductive side and circular shape radius of 20 mm and thickness $h = 1.524$ mm. The unit cell has the rectangular

shape, inspired by the works [21-23], with insertion of a small circle with radius $R = 1$ mm. Fig. 4 illustrates the unit cell and the periodic arrangement of the proposed metasurface. The dimensions of the unit cell are: L1 = 8.0 mm, L2 = 1.0 mm, S1 = 11 mm, and S2 = 5 mm.

The proposed structure is designed by coupling the copper-free side of the metasurface to the top of the microstrip antenna and in direct contact with it, thus preventing air gap formation. As illustrated in Fig. 5. We used Teflon screws, which tightened the meta-surface and the antenna, without leaving an air layer between them.

It is important to show that the proposed cell behaves as a metamaterial in the frequency range of interest. Thus, we use the methodology proposed in [24], which uses an S-parameter retrieval method to characterize artificially structured metamaterials. In this method, the unit cell S-parameters are obtained with the ANSYS HFSS and, according to the equations provided in [24], are used to obtain the electrical permittivity, magnetic permeability and refractive index. The excitation used was the Wave Port type. It is equivalent to a semi-infinite waveguide that will excite the structure with an incident wave perpendicular to the surface. The retrieved material parameters are illustrated in Fig. 6. The retrieved index is illustrated in Fig. 6(a) and it confirms the negative index band that lies between roughly 1 GHz and 9.5 GHz. Using the impedance and index we find functional forms for the permittivity and permeability, as shown in Fig. 6(b) and (c), respectively.
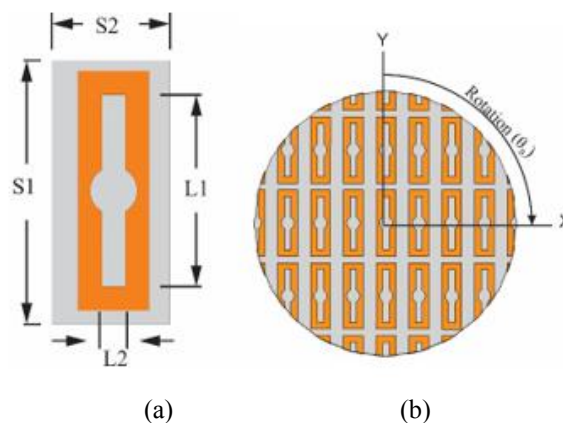


(a)                         (b)

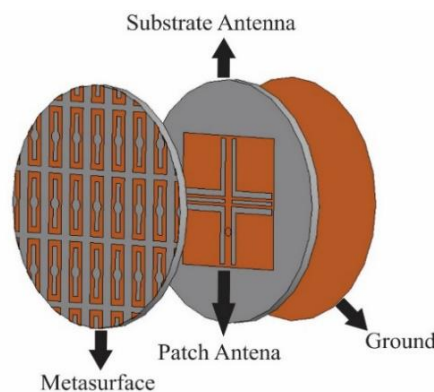Fig. 4. Geometry: (a) unit cell and (b) metasurface.
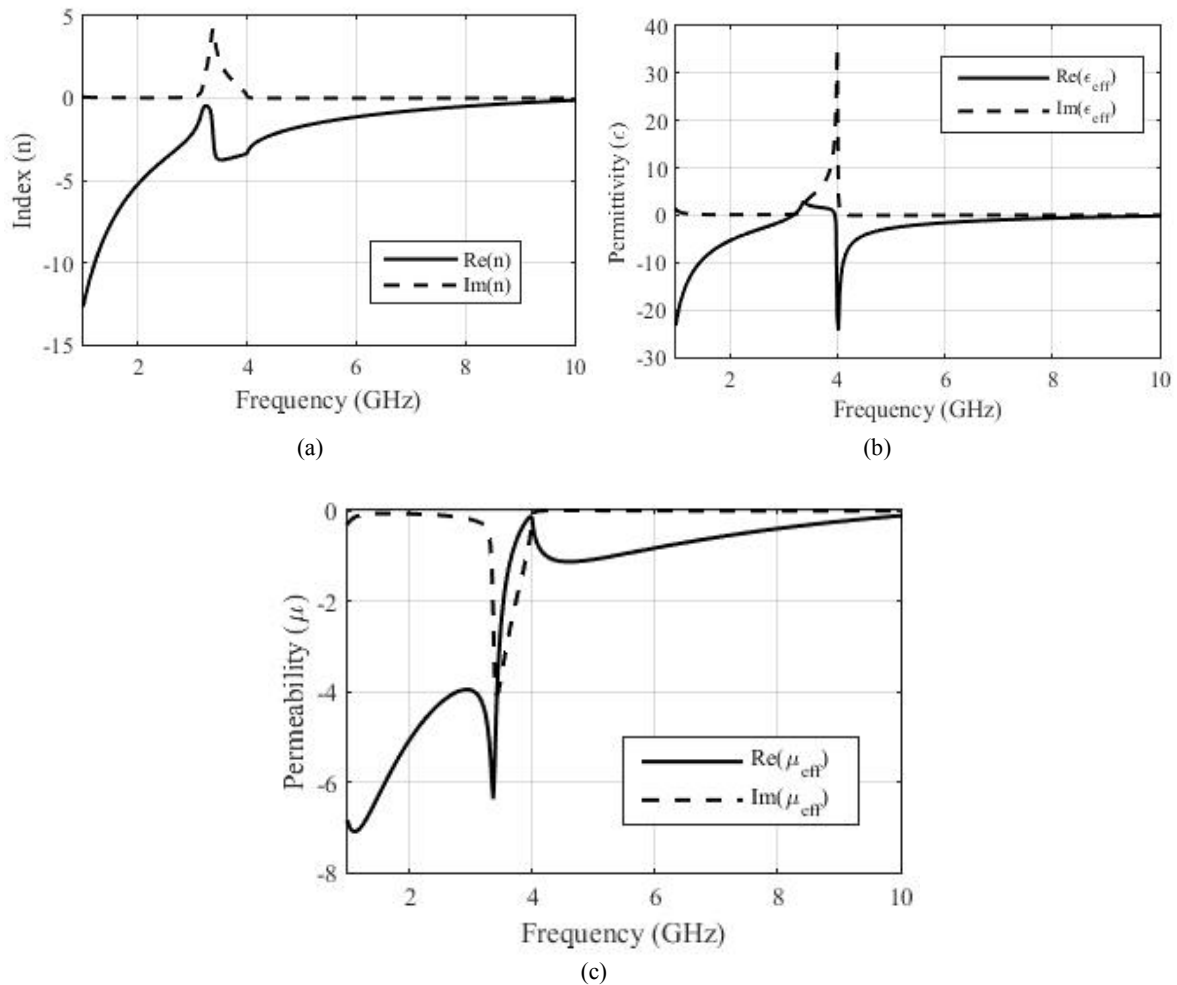


Fig. 5. Proposed structure.

Fig. 6. The retrieved material parameters: (a) index, (b) permittivity, and (c) permeability.

It is observed that the real part of the refractive index, permittivity and permeability are negative at every frequency of interest, which justifies that the unit surface meta-cell acts as a DNG material or left handed material.

## IV. PARAMETRIC ANALYSIS

To analyze the effect of metasurface on the antenna resonant s, we plotted the S11 response to the antenna without the metasurface and with the metasurface, as shown in Fig. 7, considering this positioning as the metasurface at 0°, Fig. 4 illustrates this situation. We can observe that the metasurface coupling inserts reactive elements to the antenna impedance reducing its resonant frequencies. The original patch antenna has 3 resonant frequencies at 2.17, 6.97 and 8.28 GHz. With the insertion of the metasurface, these resonant frequencies were shifted to 1.86, 6.43 and 7.42 GHz. 7.83 and 8.69 GHz. We can observe the appearance of three new resonant frequencies at 6.97, 7.83 e 8.69 GHz.
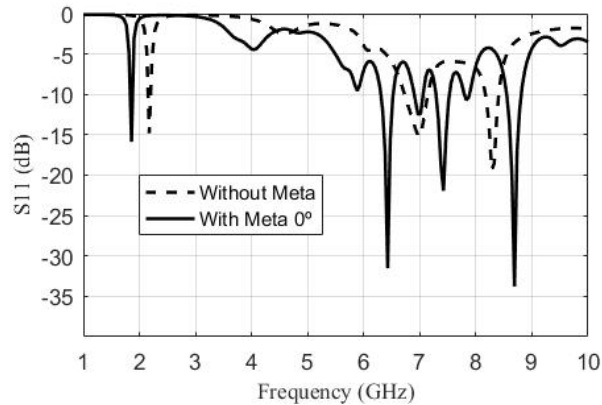
Fig. 7. Comparison of S11 for antenna with and without the use of metasurface.

Beginning the parametric analysis, clockwise meta-surface rotations were performed to obtain an optimal angle in which the resonant frequencies overlap, increasing the bandwidth in the range of interest. Fig. 8 illustrates the frequency response of $|S_{11}|$ for angles of 0°, 30° and 60°. We can see that as we increase the rotation angle the resonant frequencies overlap so that at 60° we get a bandwidth of approximately 3.5 GHz.
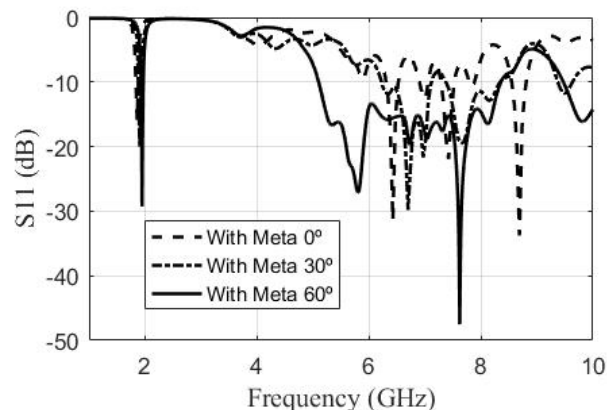


Fig. 8    Comparison of $S_{11}$ for different metasurface rotation angles.

In [21] and [22] the authors state that the meta-surface (MS) can be considered as a special dielectric that has a variable relative permittivity when illuminated by a linearly polarized plane wave. The permittivity value depends on the direction of the polarization of the plane wave. However, we understand that the MS has a variable impedance, whose real and imaginary parts depend on the direction of the polarization of the plane wave. Fig. 9(a) and (b) illustrate real and imaginary parts of the antenna with and without MS. We can see in Fig 9(a) that the real part of the antenna impedance without MS has a value greater than 50 Ω from 5.3 to 5.8 GHz, while the imaginary part, according to Fig. 9(b), varies from − 300 to 100 Ω. From 5.8 to 8 GHz, the imaginary part ranges from approximately − 300 to 70 Ω, whereas at 6.97 GHz, the real part is close to 50 Ω and the imaginary part is close to zero, resulting in the resonant frequency that we observed in Fig. 7. When we rotate

the MS, the total impedance of the set, antenna + MS, gets the real part equal to 50 Ω, while the imaginary part approaches zero. Until in 60° this happens. So, the admittance of the metasurface in combination with the admittance of the antenna allow the excitation of new resonant frequencies.
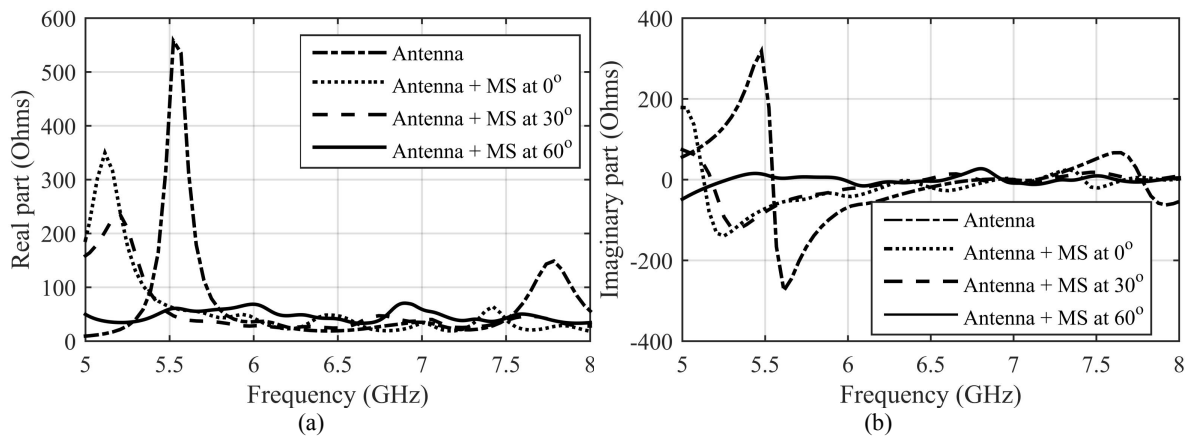


Fig. 9. Total impedance of antenna and antenna + MS: (a) real part and (b) imaginary part.

We also simulate the current distribution for the first and last resonant frequency in the band of interesting, 5.4 GHz and 7.4 GHz, respectively. As we can see in Fig. 10, without metasurface the antenna has a low current distribution. With the metasurface, the antenna presents a very high current distribution, showing that it is resonating at those frequencies.
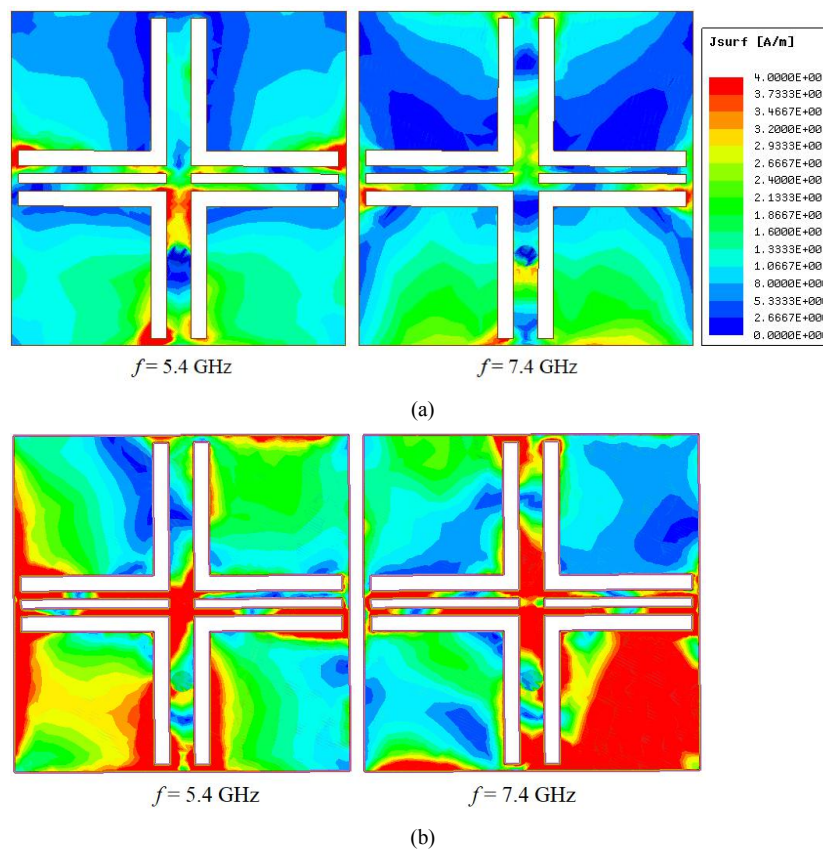


Fig. 10. Current distributions: (a) Antenna without metasurface and (b) Antenna with metasurface.

To further optimize the response obtained, a parametric analysis of the physical dimensions of the meta-surface unit cell was performed. In this analysis, we vary only one physical parameter at a time. The slot width in the unit cell (L2) together with the length (L1) were investigated to determine an optimal constructive value. Fig. 11 illustrates the results for L2 = 1.0 mm by varying the dimension of L1. As the length of the slot increases, there is a greater overlap of resonant frequencies and therefore a greater bandwidth. Thus, we have the optimal constructive value L1 = 8 mm.

Fig. 12 provides the results for L1 = 8 mm by varying the dimensions of L2. The variation in slot width (L2) does not substantially change the impedance bandwidth and to facilitate construction, as an integer value, L2 = 1.0 mm is adopted. The values of S1 and S2 corresponding to the periodicity of unit cells were limited by available technology.
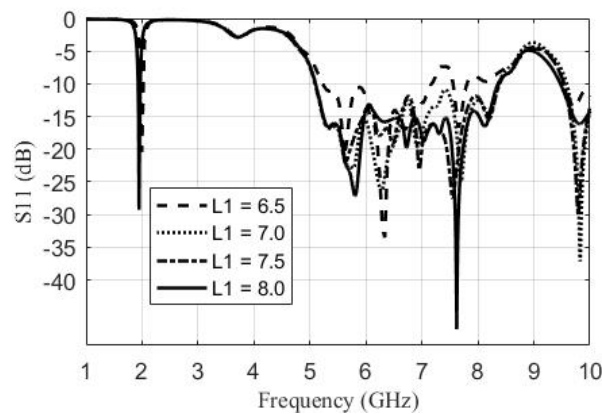


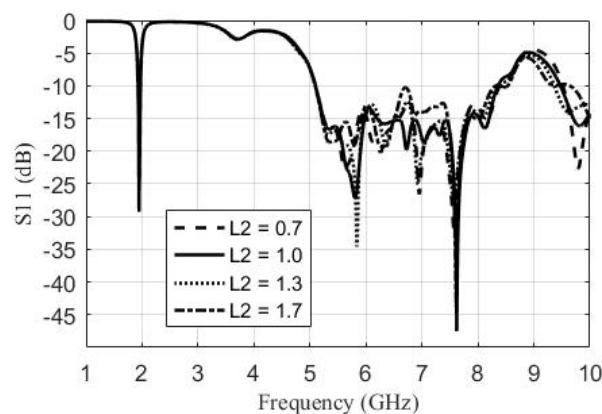Fig. 11. Comparison of $S_{11}$ for different values of L1.



Fig. 12. Comparison of $S_{11}$ for different values of L2.

V. NUMERICAL AND EXPERIMENTAL RESULTS

This section will present some simulations parameters and compare some simulated results (ANSYS HFSS) with measured (Agilent Vector Network Analyzer) to validate the new metasurface configuration capable of enhance the bandwidth of a microstrip antenna. The dimensions used in manufacturing were described in Section 3. Fig. 13(a) shows a prototype photograph of the manufactured antenna and Fig. 13(b) the Measurement Setup.

<center>(a)</center><center>(b)</center>
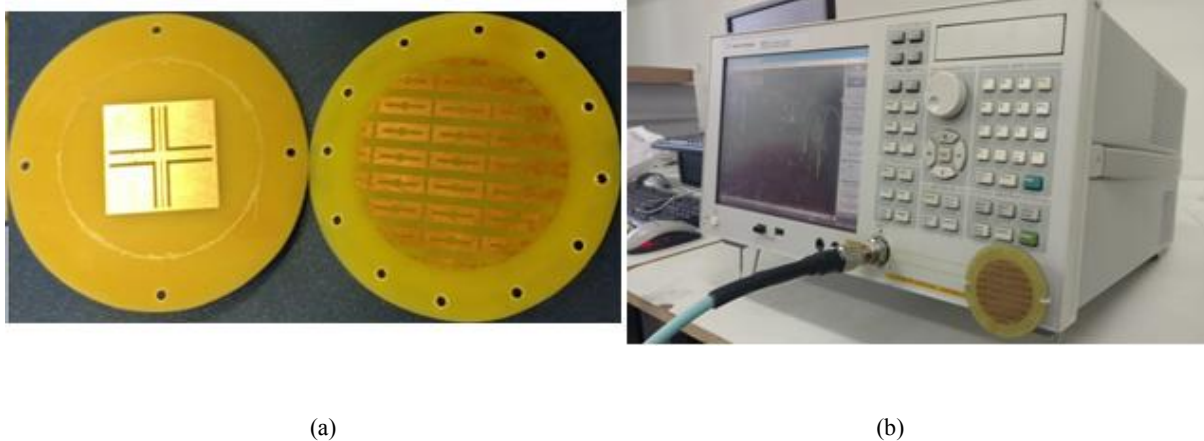
<center>Fig. 13. Photos of: (a) Antenna and metasurface and (b) VNA measurement.</center>

Fig. 14 compares the measured and simulated results of the 60° rotational metasurface (MS) coupled antenna (consider 0° as MS position in Fig. 4) clockwise of the MS around the axis itself. It can be observed that the simulated and measured results are in good agreement, although there may be some discrepancies between experimental and simulation results due to manufacturing tolerances and variations in the characteristics of the material used.
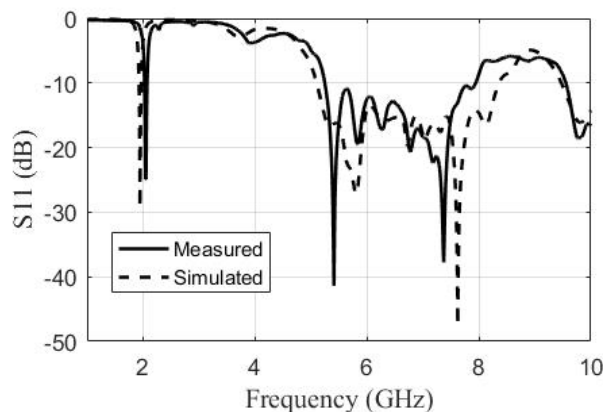


<center>Fig. 14. Comparison between simulated and measured results for metasurface at 60º.</center>

Fig. 15 shows comparison between simulated and measured gain. As we can see, a good agreement between results is observed. We limited the observation for the interesting frequency range. The frequency range comes from 5.1 GHz to 7.2 GHz, which is the band for WiFi 5 and 6. The simulated gain is the dashed line and the measured gain is the solid line. The gain was simulated for Phi = 0 and Theta = 0 using HFSS. The mean gain simulated is 2.98 dBi while the measured mean gain is 2.74 dBi. The gain was measured using an Agilent E5071C two ports network analyzer and two calibrated SAS-571 double ridge guide horn antennas with a known gain, positioned at a distance of 50 cm. We measured the $S_{21}$. After this, we changed one of the antennas by our proposed antenna and repeat the measurement. From the $S_{21}$, the distance, and the gain known of the horn antenna, we calculated the gain of our antenna. We think that the deviation between the gains from 6.6 GHz to 6.8 GHz occurs

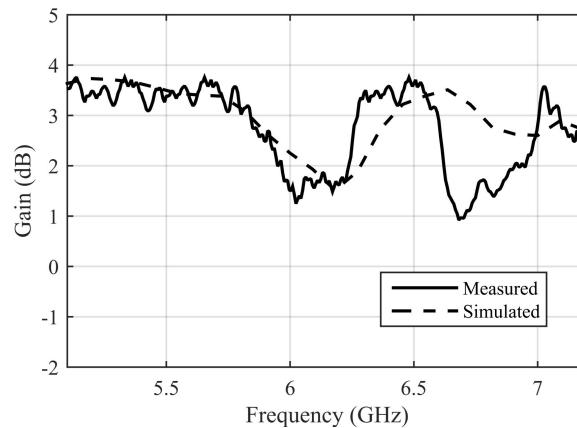because the measurements were not performed in an anechoic chamber.



Fig. 15. Comparison between simulated and measured gain for range from 5.1 GHz to 7.2 GHz.

Some important parameters were simulated to show how the MS improved the response of the antenna. One of these parameters was the efficiency. Fig. 16 shows how the efficiency changes for different rotation angles. The efficiency improved in all bandwidth when we rotate the MS. The mean efficiency was 48 % for 0° and improved for 58 % for 60°.
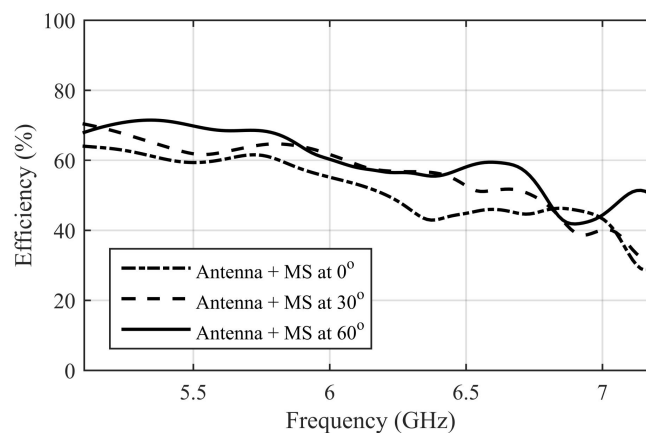


Fig. 16. Comparison between simulated and measured gain for range from 5.1 GHz to 7.2 GHz.

Another important parameter is the radiation pattern, as illustrated in Fig 17. It is important that the diagram undergoes few changes over the entire band. Thus, we plot the diagrams on the E and H planes, for the frequencies of 5.5 GHz and 6.5 GHz. We can notice that the radiation patterns undergo little change along the band, both on the XZ-plane, and in the YZ-plane. Also, we can have noticed that the antenna has no polarization purity, but it is not a circular polarized antenna.
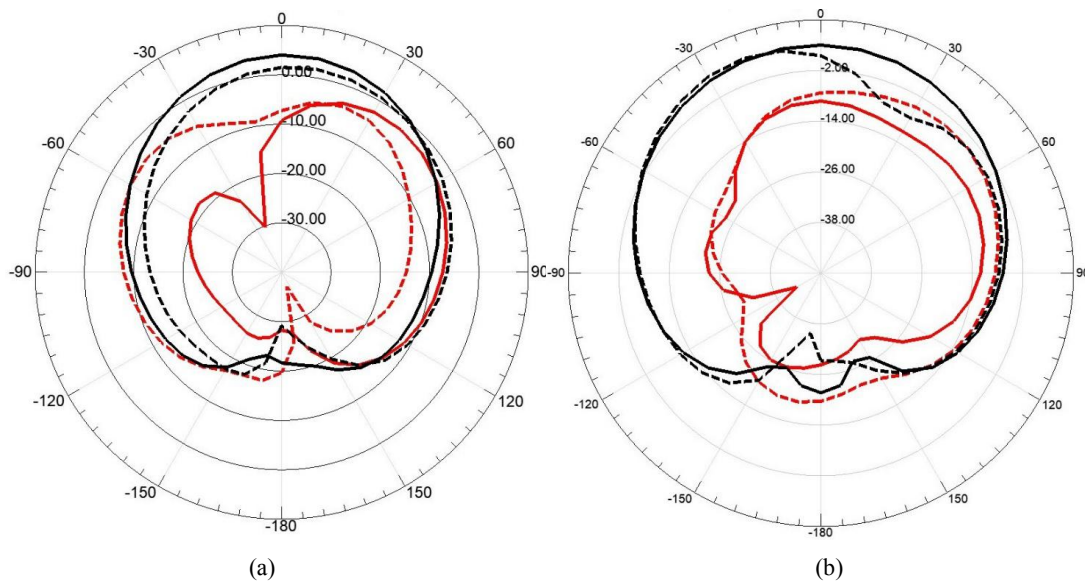
Fig. 17. Radiation pattern of Co- (black line) and Cross-polarization (red line): (a) XZ-plane and (b) YZ-plane (---) 6.5 GHz and (—) 5.5 GHz.

## VI. CONCLUSIONS

In this work, we propose the use of a metasurface coupled to a microstrip patch antenna for bandwidth enhancement. The final volume of the antenna was 3.82 cm$^3$. The metasurface was rotated until the largest fractional bandwidth was obtained, whose best angle was 60°. The set can be used for WiFi 5 and 6 applications. The final fractional bandwidth was 45.4 % (5.1 – 8.0 GHz) and the peak gain was 3.8 dBi. The square patch antenna and the metasurface were built for validation purposes. It can be observed that the simulated and measured results are in good agreement.

## REFERENCES

[1] K. Goodwilll, N Singh, and M. V. Kartikeyan, "Dual band circular polarized bow tie slotted patch antenna over high impedance surface for WiMAX application", *International Journal of Microwave and Wireless Technologies*, vol. 12, pp. 303–308, 2020.

[2] M. S. Ellis et al., "Asymmetric circularly polarized open-slot antenna", *International Journal of RF Microwave Computer Aided Engineering*, vol. 30, no. 5, pp. 1 – 10, 2020.

[3] W. An et al., "Low-profile and wideband dipole antenna with unidirectional radiation pattern for 5G", *IEICE Electronics Express*, vol. 15, no. 13, pp. 1 – 6, 2018.

[4] M. Bjelogrlic et al., "Stratified spherical model for microwave imaging of the brain: Analysis and experimental validation of transmitted power", *Microwave and Optical Technology Letters*, vol. 60, pp. 1042 – 1048, 2018.

[5] S. Banerjee and S. K. Parui, "Bandwidth improvement of substrate integrated waveguide cavity-backed slot antenna with dielectric resonators", *Microsystem Technology*, vol. 26, pp. 1359 – 1368, 2020.

[6] Y. Cheng, et al., "Design and Analysis of a Bow-Tie Slot-Coupled Wideband Metasurface Antenna", *IEEE Antennas and Wireless Propagation Letter*s, vol. 18, no. 7, pp. 1342 – 1346, 2019.

[7] A. Verma et al., "Slot loaded EBG-based metasurface for performance improvement of circularly polarized antenna for WiMAX applications", *International Journal of Microwave and Wireless Technologies*, vol. 12, pp. 212 – 220, 2020.

[8] B. A. Mouris et al., "On the Increment of the Bandwidth of Mushroom-Type EBG Structures with Glide Symmetry", *IEEE Transactions on Microwave Theory and Techniques*, vol. 68, no. 4, pp. 1365 – 1375, 2020.

[9] O. Sokunbi and H. Attia, "Highly reduced mutual coupling between wideband patch antenna array using multiresonance EBG structure and defective ground surface", *Microwave and Optical Technology Letter*s, vol. 62, no. 4, pp. 1628 – 1637, 2020.

[10] S. S. Bukhari, J. Vardaxoglou, and W. Whittow, "A Metasurfaces Review: Definitions and Applications", Application Science, vol. 9, no. 13, pp. 1 – 14, 2019.

[11] Z. Yang et al., "Metasurface-based wideband, low-profile, and high-gain antenna", *IET Microwaves, Antennas & Propagation*, vol. 13, no. 4, pp. 436 – 441, 2019.

[12] M. A. Rad, M. R. Soheilifar, and F. B. Zarrabi, "Compact microstrip antenna based on fractal metasurface with low radar cross section and wide bandwidth", *AEU - International Journal of Electronics and Communcatio*ns, vol. 98, pp. 74 – 79, 2019.

[13] N. Nie, X. Yang, Z. N. Chen, and B. Wang, "A Low-Profile Wideband Hybrid Metasurface Antenna Array for 5G and WiFi Systems", *IEEE Transactions on Antennas and Propagation*, vol. 68, no. 2, pp. 665 – 671, 2020.

[14] X. Deng, X. Xu, and J. Wei, "Characterization of extremely low profile patch antenna loaded with periodic diamond metasurface ground plane", *Microwave and Optical Technology Letters*, vol. 62, no. 4, pp. 1774 – 1779, 2020.

[15] J. Dong, C. Ding, and J. Mo, "A Low-Profile Wideband Linear-to-Circular Polarization Conversion Slot Antenna Using Metasurface", *Materials*, vol. 13, no. 1164, pp. 1 – 12, 2020.

[16] R. P. Pravin, "Multilayered Circularly Polarized Microstrip Antenna Integrated with Defected Ground Structure for Wide Impedance and Axial Ratio Bandwidth", *Journal of Electromagnetic Waves and Applications*, vol. 17, no. 30, pp. 2256–2267, 2016.

[17] V. S. Aravind, G. Shilpi, B. S. Satya, K. K. Mukundan, and C. K. Aswathi, "Compact EBG Ground Plane Microstrip Antenna for Broad Bandwidth Applications", Microwave and Optical Technology Letters, vol. 3, no. 58, pp. 555-557, 2016.

[18] M. A. Rad, M. R. Soheilifar, and F. B. Zarrabi, "Compact Microstrip Antenna Based on Fractal Metasurface with Low Radar Cross Section and Wide Bandwidth", *International Journal of Electronics and Communication*s, vol. 98, pp. 74–79, 2018.

[19] A. Agrawal, P. K. Singhal, and A. Jain, "Design and Optimization of a Microstrip Patch Antenna for Increased Bandwidth", *International Journal of Microwave and Wireless Technologies*, vol. 5, no. 4, pp. 529–535, 2013.

[20] S. Kumar, and D. K. Vishwakarma, "Miniaturized Bent Slotted Patch Antenna Over a Reactive Impedance Surface Substrate", *International Journal of Microwave and Wireless Technologies*, Vvol. 8, no. 2, pp. 347–352, 2016.

[21] H. L. Zhu, S. W. Cheung, and T. I. Yuk, "Frequency-Reconfigurable Slot Antenna with Wide-Tuning Range Using Metasurface", *Microwave and Optical Technology Letters*, vol. 6, no. 57, pp. 1475-1481, 2015.

[22] H. L. Zhu, X. H. Liu, S. W. Cheung, and T. I. Yuk, "Frequency-Reconfigurable Antenna Using Metasurface", *IEEE Transactions on Antennas and Propagation*, vol. 1, no. 62, pp. 80-85, 2014.

[23] B. Majumder, K. Kandasamy, J. Mukherjee, and K. P. Ray, "Wideband Compact Directive Metasurface Enabled Pair of Slot Antenas", *Electronics Letters*, vol. 17, no. 51, pp. 1310–1312, 2015.

[24] D. R. Smith, D. C. Vier, T. Koschny., and C. M. Soukoulis, "Electromagnetic parameter retrieval from inhomogeneous metamaterials", *Physical Review E*, vol. 3, no. 71, pp. 36617-11, 2005.